Compact Size MIMO Amer Fractal Slot Antenna for 3G, LTE (4G), WLAN, WiMAX, ISM and 5G Communications

AMER TAWFEEQ ABED [1], (Member, IEEE), **AND AQEEL MAHMOOD JAWAD** [2]

[1]Department of Communication Engineering, Al-Ma'moon University College, Baghdad, Iraq
[2]Department of Computer Communication Engineering, Al-Rafidain University College, Baghdad, Iraq

Corresponding author: Amer Tawfeeq Abed (amer.t.abed@ieee.org)

ABSTRACT In this study, an Amer fractal slot antenna is proposed as a multiple input, multiple output (MIMO) antenna with four ports. The antenna is excited by CPW (coplanar waveguide) to control the leakage of electromagnetic energy, which leads to a high match between the antenna and input impedance, thus achieving dual operating bands of 1.5-19.2 GHz and 25-37.2 GHz for port 1, dual operating bands of 1.4-19 GHz and 20-35.5 GHz for port 2, a wide operating band of 1.4-29 GHz for port 3, and dual operating bands of 1.6-21 GHz and 22-37 GHz for port 4. Therefore, the proposed antenna meets all the market needs of wireless communication technologies such as 3G, Long Term Evolution (LTE, 2.6 GHz /3.5 GHz), Wireless Local Area Network (WLAN, 2.4 GHz/5 GHz), Worldwide Interoperability for Microwave Access (WiMAX, 2.5 GHz/3.5 GHz/5 GHz), Industrial, Scientific and Medical (ISM, 2.4 GHz/ 5 GHz), and 5G (5-6 GHz and 27-28 GHz). The proposed antenna can be used as dual opposite ports for the frequency range 1.5-15 GHz and as four-element MIMO arrays for frequencies of 15-30 GHz. The MIMO fractal antenna has circular polarization characteristics with axial ratio bandwidths (ARBWs) of 4.7-5.8 GHz for port 1, 2.5-2.6 GHz and 5.4-6.5 GHz for the port 2, 4-5.9 GHz for port 3, and 5.5-10 GHz for port 4. Due to its compact size (33 mm × 33 mm × 0.8 mm), low profile, and acceptable values of gain and efficiency, the proposed antenna is suitable for many portable wireless communication devices.

INDEX TERMS Fractal slot, MIMO antenna, LTE and 5G.

I. INTRODUCTION

Multiple input, multiple output (MIMO) antennas are used for improved wireless channel capacity. The adopted MIMO technology provides an effective, high data rate that is split into multiple lower-rate streams for spatial diversity characteristics. MIMO antennas are used to support many wireless communication technologies, such as WLAN, 3G, LTE, and WiMAX (4G) [1]. Many researchers have designed MIMO antennas that have different shapes and cover various frequency bands [2]–[24]. The headings in Table I indicate important specifications, such as number of elements, impedance bandwidth (BW), efficiency, gain, mutual coupling, axial-ratio bandwidth (ARBW), and size, as well as

The associate editor coordinating the review of this manuscript and approving it for publication was Sudipta Chattopadhyay.

weak points for all related antennas [2]–[24]. The table shows that one problem shared by most previous antennas is linear polarization radiation. However, certain antennas in Table-I have circularly polarized radiation, such as [3], which proposed three radiator elements that have an overall size of 48 mm × 29 mm × 1.6 mm and a narrow ARBW that is approximately 15% of the operating band 5-6 GHz. In [10], the 3.6-3.65 GHz ARBW is narrow but has used all available antenna operating bands. Some of the operating bands are not useful for wireless communication because their bandwidths are less than 100 MHz. In [12], dual substrates (Rogers 5880, Rogers 3006) were used to design a MIMO antenna with four elements in a compact size with an ARBW of 30.5-32 GHz, which is about 30% of the operating band of 29-34 GHz. However, that antenna cannot support 3G, LTE, WLAN, WIMAX, and ISM. The highly

TABLE 1. Comparison of antennas reported in [2]–[24].

Ant.	No El.	BW (GHz)	Effie. %	Gain (dBi)	ARBW (GHz)	ECC	S_{ij} (dB)	Size (mm)	Weak points
[2]	4	(2.3-2.9)	80-90	0~5	LP	-	< −10	91x91x0.8	LP, large size, missed many required bands.
[3]	3	(5-6)	55-60	-2~2	5.6-5.75	0.15	< −15	48x29x1.6	Missed many required bands
[4]	16	(5-6)	70-80	-	LP	0.1	< −10	30x30x13	LP, missed many required bands
[5]	2	(2.4-2.5) (5-6)	-	-	LP	0.1	< −25	77x34x0.8	LP, missed many required bands
[6]	2	(4-6.5)	80	4~7	LP	0.05	< −15	80x50x0.76	LP, missed many required bands
[7]	4	(1.8-2.5)	51-73	- 2.6~2.4	LP	0.1	< −10	120x60x0.7	LP, missed many required bands
[8]	4	(2.15-2.33)	75-85	-	LP	0.25	< −11	100x60x0.8	LP, large size, missed many required bands
[9]	4	(27.5-28.5)	-	-	LP	0.05	< −30	130x70x2.2	LP, large size, missed many required bands
[10]	2	(0.9-1) (1.7-1.77) (2.6-2.8) (4.2-4.4) (5.5-5.65)	-	2.5~ 6.5	3.6-3.65	0.05	< −17	82x40x0.8	Narrow ARBW, lower operating bands less than 100MHz
[11]	2	(3-10.5)	40-82	2~5.5	LP	0.42	< −15	24.3x22x0.8	LP, low efficiency values at lower band.
[12]	4	(29-34)	-	-	30.5-32	-	< −20	30x30x3	Missed many required bands
[13]	8	(3-15)	50-80	0~3	LP	0.2	< −10	90x38x0.76	LP, large size, missed 2.4-2.7 GHz band.
[14]	2	(2.4-2.48) (5.15-5.825)	60-80	-	LP	0.05	< −15	77.5x52x1.6	LP, there are no gain values
[15]	4	(1.95-2.5) (3.15-3.85) (4.95-6.6)	60-80	-1~2	LP	0.2	< −15	40x40x1.6	LP, low gain at lower band.
[16]	2	(1,8-2.5) (26.-28.5)	-	1.5~3.5	LP	-	< −10	100x60x0.9	LP, large size, missed many required bands.
[17]	4	(2.6-2.8) (3.4-3.6)	-	2 ~4	LP	0.4	< −16	140x 70x 9.5	LP, large size, missed band of 5-6 GHz.
[18]	4	(3-9)	60-85	0.5 ~2	LP	0.1	< −10	40x40x0.8	LP, missed band of 24-2.7 GHz.
[19]	2	(1.9-3.7)	-	-0.5 ~6	LP	0.06	< −15	100x50x1.6	LP, large size, missed many required bands.
[20]	4	(5.1-5.35)	-	-	LP	0.2	< −10	130x10x0.8	Large size, LP, missed many required bands.
[21]	2	(0.1-4.3)	56	-1 ~ 3.1	2.2-3.2	0.03	< −30	8 × 8 × 0.8	Low gain & efficiency at lower band, missed band of 5-6 GHz
[22]	2	(8.7-11.7) (11-14) (15.6-17.1) (29-34)	70-90	5 ~9	LP	-	< −27	70x37x1.6	Missed many required bands, LP
[23]	4	(8-9.25)	77-84	2 ~6	LP	-	< −32	120x90x15	LP, Missed many required bands, large size, big edge-to-edge gap
[24]	2	(2.64-2.68)	68	-	LP	0.23	< −40	68x40x1.6	Narrow operating band, LP, missed many required bands.

compact fractal antenna investigated in [21] has an ARBW of 2.2-3.2 GHz, which is approximately 23% of the operating band of 0.1-4.3 GHz.

However, this antenna has low gain values at lower bands and low efficiency. The antennas reported in [2], [7], [8], [9], [13], [16], [17], [19], [20], and [23] are large and thus cannot be used in modern portable communication devices. Conversely, previous antennas that are small in size also have low efficiency or gain, such as [4], [5], [10], [12], and [21]. In [22], the MIMO antenna missed many required bands and cannot be used for 3G, LTE, WLAN, WiMAX and ISM, while [24] has a narrow, linearly polarized operating band that can support LTE / 2.6 GHz only.

Therefore, it is nedded to design a MIMO antenna with a compact size, high gain and efficiency, and CP radiation, with a wide impedance bandwidth that can be used for many wireless communication devices.

This research aims to design a compact dual-opposite-port MIMO fractal slot antenna that has a wide impedance bandwidth that can be used for 3G, LTE, WLAN, WiMAX, ISM, and 5G applications; acceptable values of efficiency and gain; circularly polarized radiation; and low mutual coupling between opposite ports at all operating bands.

II. ANTENNA DESIGN AND ANALYSIS

A. ANTENNA DESIGN

Figures 1a and 1b show the process of antenna configuration. The initiator antenna consists of the radiator with dimensions of $23d \times 23d$ and the ground (Fig.1a). The ground and the radiation plates are on the same side of the dielectric; thus, the antenna is coplanar. The antenna is fed by four CPW ports for two purposes. First, it must control the leakage of the electromagnetic energy by optimizing the gap g_1 between the feeding line F and the ground plate. Second, it must be able to optimize the match between the antenna and the input impedance (50Ω), because the impedance of the CPW depends on the width of feeding F and the gap g_1. The dimensions of the feeding line F are selected and optimized to be $5d \times 1.5d$ for all ports, $g_1 = 0.25d$ is the gap between the feeding line F and the ground plate. The radiating element is separated from the ground plate by a gap $g_2 = 0.5d$.

At the second step, an Amer fractal slot [25] etched on the radiator plate of the initiator to configure the proposed antenna as it is shown in Fig.1b. The proposed antenna printed on a commercial FR-4 substrate measuring 33 mm $\times$ 33 mm, with a thickness of 0.8 mm. The width of the fractal slot is d. All dimensions in the figure 1 are defined by d, where d = 1mm. The positions of the ports are selected by use of the software CST such that a wide impedance bandwidth is generated.

Figure 2 depicts the values of S_{11}, $S_{22}S_{33}$ and S_{44} for the proposed MIMO antenna with (the solid curves) and without (the dotted curves) Amer fractal slot. The black and red dotted curves in Fig.2a indicate that the initiator antenna (without Amer fractal slot) has narrow impedance bandwidth
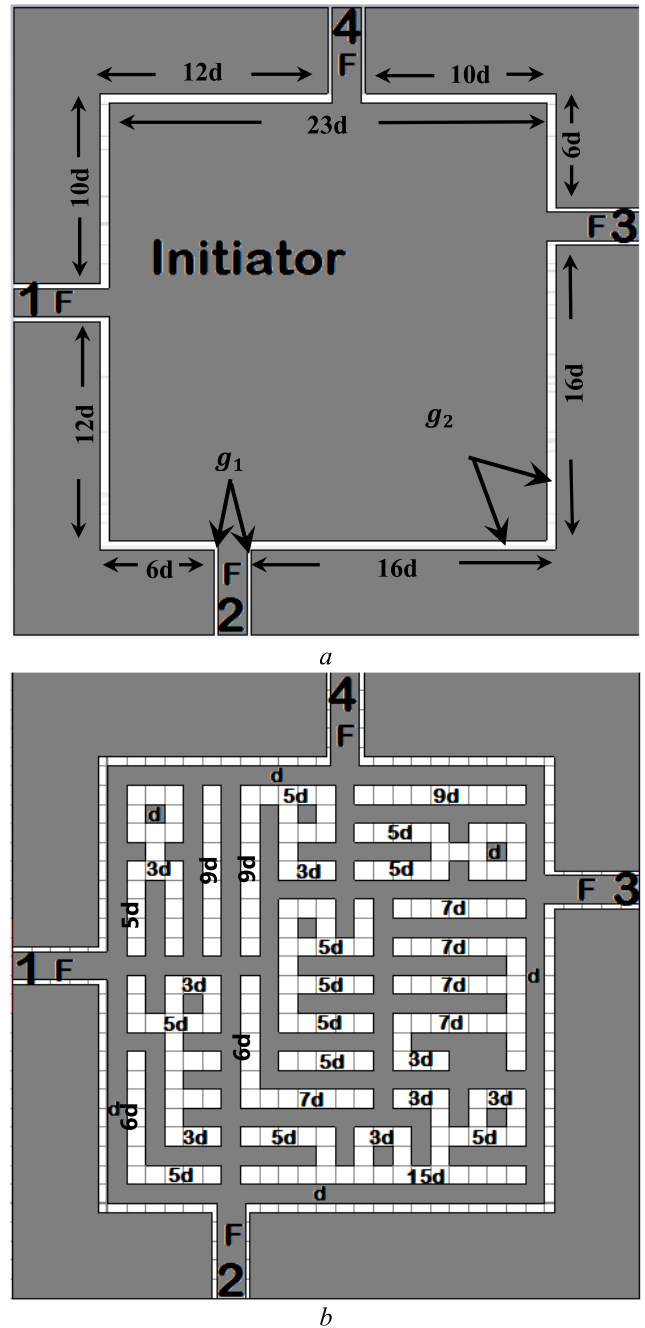

FIGURE 1. The geometry of MIMO Amer fractal slot antenna (d = 1mm). a. The initiator. b. Amer fractal slot.

of 27.5-28.7GHz for port1 and port4, while the proposed antenna with Amer fractal slot has a wide impedance bandwidth of 1.5-37 GHz for pot1(the black solid curve in Fig.2a) and 1.5-10.3 GHz, 10.6-39.3 GHz for port 4 (the solid red curve in Fig.2a).

The impedance bandwidth of the proposed antenna enhanced to 1.35-36 GHz for port2 (the black solid curve in Fig.2b) and 1.3-30 GHz for port3 (the red solid curve in Fig.2b) compared with the impedance bandwidths of 7.1-7.5GHz and 27.5-28.5 GHz for port2 and port 3 (the black and red doted curves in Fig.2b). The impedance
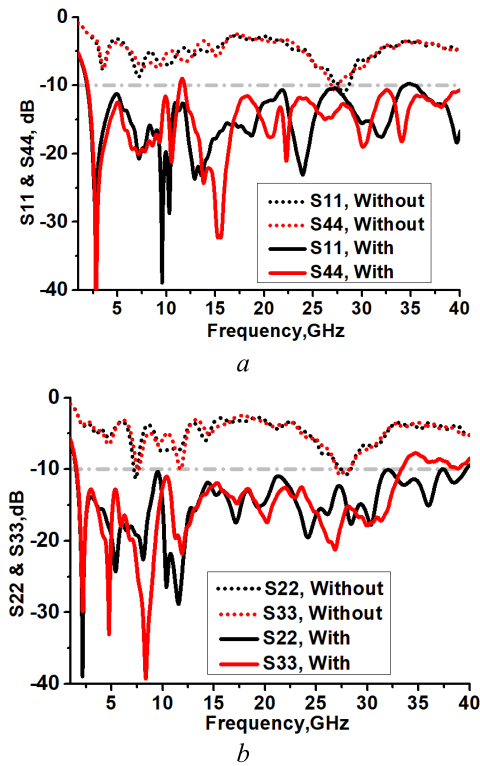
FIGURE 2. Simulated S_{11}, S_{22}, S_{33} and S_{44} for the proposed antenna with and without Amer fractal slot.
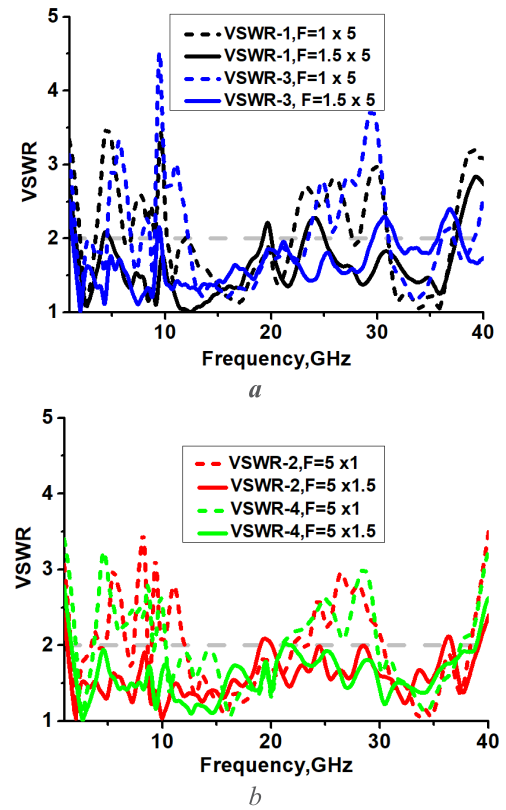

FIGURE 3. Equivalent circuit of the proposed MIMO antenna.

FIGURE 4. Simulated VSWR when varying the width of fed line.

ports excited and can be calculated as [26]:

$$V_{1,2,3,4} = I_1 Z_{11} + I_2 Z_{12} + I_3 Z_{13} + I_4 Z_{14} \qquad (1)$$

$$V_{2,1,3,4} = I_2 Z_{22} + I_1 Z_{21} + I_3 Z_{23} + I_4 Z_{24} \qquad (2)$$

$$V_{3,1,2,4} = I_3 Z_{33} + I_1 Z_{31} + I_2 Z_{32} + I_4 Z_{34} \qquad (3)$$

$$V_{4,1,2,3} = I_4 Z_{44} + I_1 Z_{41} + I_2 Z_{42} + I_3 Z_{43} \qquad (4)$$

where $Z_{11} = r_{1rad} + r_{1loss}$, $Z_{22} = r_{2rad} + r_{2loss}$, $Z_{33} = r_{3rad} + r_{3loss}$ and $Z_{44} = r_{4rad} + r_{4\,loss}$. Since all ports connected to (SMA), the load impedance Z_L supposed to be 50 Ω for all ports as shown in Fig.3. When one port excited the load impedance for the other ports become as loss resistance. The radiation efficiency (E_{rad}) equals to the ratio of the radiated power (P_{rad}) to the input power (P_{in}) which can be calculated as:

$$E_{rad} = \frac{P_{rad}}{P_{in}} = \frac{P_{rad}}{P_{rad} + P_{loss}} \qquad (5)$$

$$P_{rad} = |I_1|^2 r_{1rad} + |I_2|^2 r_{2rad} + |I_3|^2 r_{3rad} + |I_4|^2 r_{4rad} \qquad (6)$$

$$P_{loss} = |I_1|^2 r_{1loss} + |I_2|^2 r_{2loss} + |I_3|^2 r_{3loss} + |I_4|^2 r_{4loss} \qquad (7)$$

Figures 4a and 4b show how the impedance of the antenna is changed by varying the width of feeding line F, which changes the gap g_1. When the width of fed line is 1mm, the impedance bandwidth of port 1 separated into the bands 2-3.2 GHz, 10-22 GHz, and 31-37 GHz (the black dashed curve in Fig.4a); the impedance for port 3 changed to 1.5-2.7 GHz, 2.9-4.4 GHz, 6.8-7.7 GHz, 8.5-9 GHz,
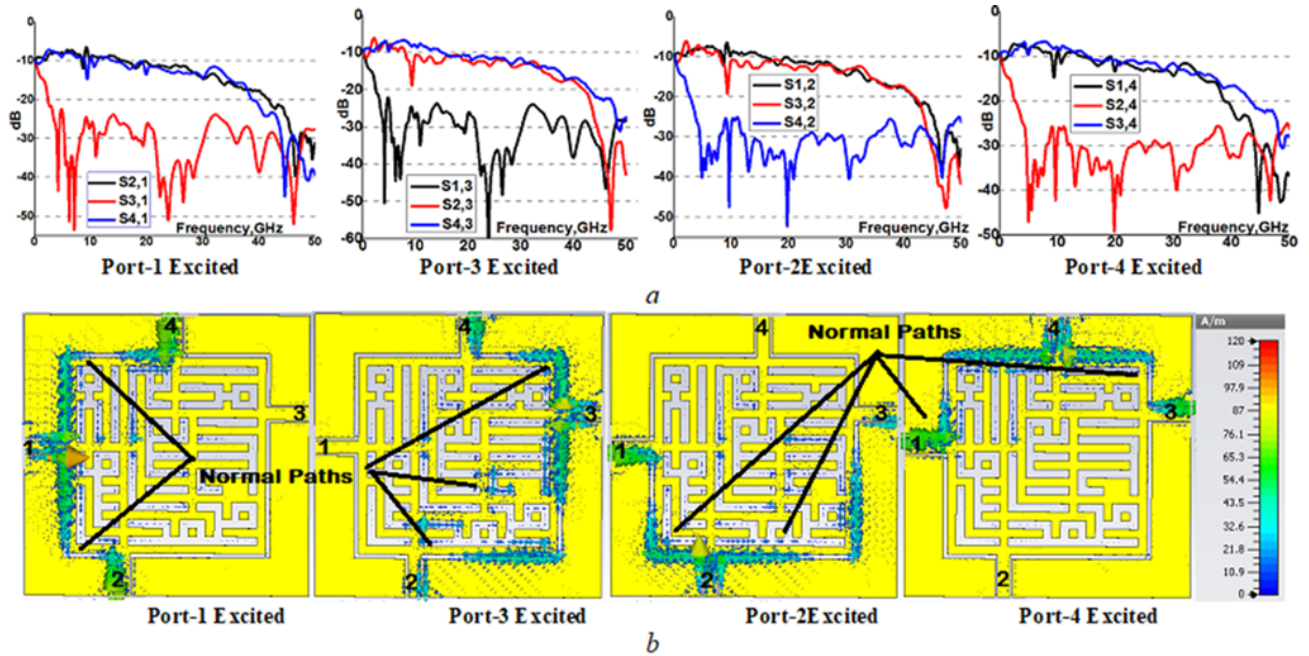
bandwidth enhanced in case of etching an Amer fractal slot in the radiator, due to the multiple paths for the surface current, where each path creates its own resonant frequencies, which together achieve a wide operating band.

Figure 3 depicts the equivalen circuit of the MIMO Amer fractal slot antenna, where Z_{11}, Z_{22}, Z_{33} and Z_{44} are the self impedance for ports 1,2,3 and 4 respictivly. $V_{1,2,3,4}$, $V_{2,1,3,4}$, $V_{3,1,2,4}$ and $V_{4,1,2,3}$ are the total mutual voltages when all

FIGURE 5. Simulated mutual coupling and surface current distribution at 5.7GHz by exciting port-1, port-3, port-2 and port-4.
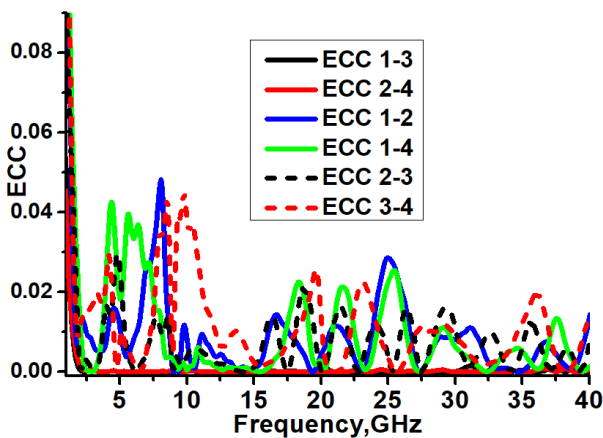

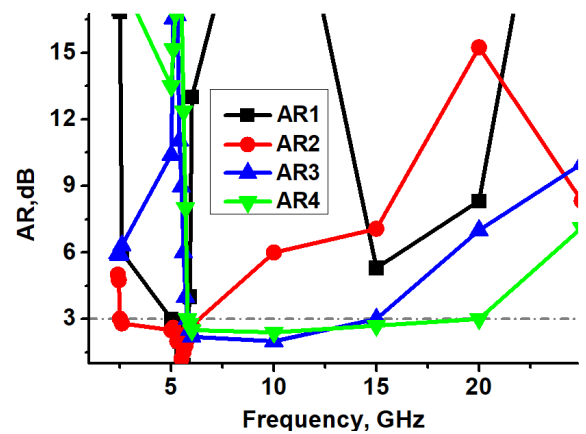**FIGURE 6.** Simulated ECC between ports (1-3), (2-4), (1-2),(1-4), (2-3) and (3-4).

FIGURE 7. Simulated AR for all ports.

13-23 GHz, and 31-35.8 GHz (the blue dashed curve in Fig.4a).The impedance bandwidth of port 2 changed to16-3.4 GHz, 6.6-7.3 GHz, 12.2-21.9 GHz, and 30.5-37 GHz (the red dashed curve in Figure 4b), while Port 4 has an impedance of 2-3.7 GHz, 10.2-21 GHz, and 30-37 GHz (the red dashed curve in Figure 4b). Therefore, the optimum dimensions of the feeding line are 5 mm × 1.5 mm and the optimum gap g_1 is 0.25 mm.

B. MUTUAL COUPLING
Figure 5 presents the mutual coupling values and current distribution when one port is excited while the others are connected to 50 ohms (SMA). When port 1 or 3 is excited, the values of $S_{3,1}$ and $S_{1,3}$ become too low (less than -22 dB), while $S_{1,2}$, $S_{4,1}$, $S_{2,3}$, and $S_{4,3}$ are -8 to -10 dB at 1-15 GHz and then decrease gradually to -20 dB at the upper band.

When port 2 or 4 is excited, the values of $S_{4,2}$ and $S_{2,4}$ are less than -10 dB at 1-15 GHz, then vary from -25 to -50 dB and mutual coupling values are high between port 2 and its neighbor ports (ports 1 and 3) for the frequency range 1.5-15 GHz. Meanwhile, for the frequency band 15-40 GHz, the mutual coupling values between all ports are less than -10 dB. Therefore, the proposed antenna can be used as MIMO by only two opposite ports (that is, either ports 1 and 3 or ports 2 and 4) at a frequency of 1.5-15 GHz. It can be used as MIMO with all four ports at 15-30 GHz, which includes 5G applications (27-29 GHz). When port 1 is excited, there is no surface current near port 3, while at ports 2 and 4 there is some surface current (see Figure5b). Conversely, there is no surface current near port 1 when port 3 is excited. The same situation happens when port 2 or port 4 is excited. At lower operating frequencies (which means longer wavelengths), the surface current needs a long path equal to one-half the wavelength
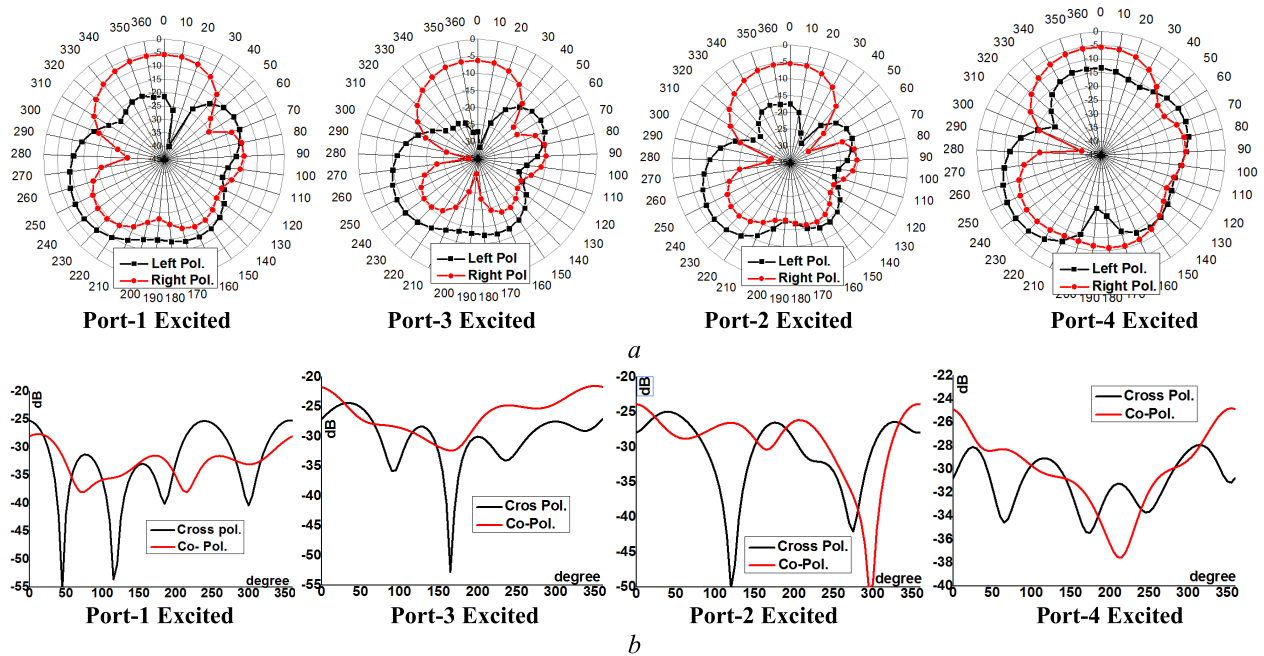
FIGURE 8. Polarization of all ports at 5.7GHz. a. Left (Black) and right (Red) polarizations. b.Cross polarization (Black) and co-polarization (Red).
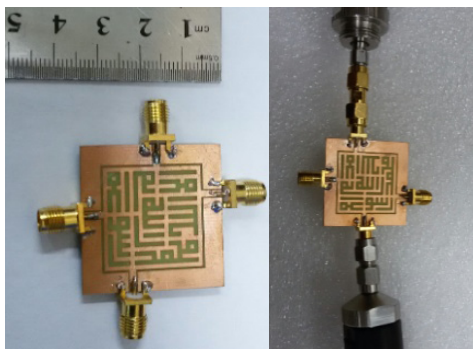

FIGURE 9. Prototype of the proposed MIMO antenna.

of the operating frequency. This long path interferes with the neighbor ports but not with the opposite port (see Figure 5b where port 1 is excited). As the operating frequency increases, the path of surface current will be short and will not interfere with the neighbor or the opposite ports. This reduces the mutual coupling with the other ports. Because there are many paths for surface current, this antenna can generate many resonant frequencies, which togather achive a wide operating band (see Figure 5b). Furthermore, multiple perpendicular paths generate dual electric fields, which make it easy for the surface current to circulate, creating CP characteristics (see Figure 5b). This is the reason for using an Amer fractal slot structure in the design.

The values of the envelope correlation coefficients (ECCs) in Figure 6 are calculated by the S-parameters according to Equation (8) [21]:

$$ECC = \frac{|S_{11}^* S_{12} + S_{21}^* S_{22}|^2}{(1 - |S_{11}|^2 - |S_{21}|^2)(1 - |S_{22}|^2 - |S_{12}|^2)} \quad (8)$$

Figure 6 shows low ECCs between ports1 and 3 (the solid black curve) and between ports 2 and 4 (the solid red curve).

Low ECCs between opposite ports match the mutual coupling values in Figure 5a and the current distribution in Figure 5b. Low ECCs between opposite ports indicate that the proposed antenna can provide good pattern diversity for all operating bands, as shown in Figure 6. The ECCs between ports 1 and 2, ports1 and 4, ports 2 and 3, and ports 3 and 4 are greater than those for the opposite ports, but still less than 0.05 (see Figure 6).

C. CIRCULAR POLARIZATION

Based on Figure 5b, the proposed MIMO antenna has perpendicular paths (which indicated by the arrows drawn in Fig.5b) for the surface current, which generate dual electric fields with a phase shift of 90^0, which is necessary for generating CP radiation. The simulated axial ratio (AR) values are presented in Figure7.

As shown in Figure 7, port 1 (the black curve) has an ARBW less than 3 dB in bands 4.8-5.1 GHz and 5.5-5.9 GHz, which are approximately 2% and 2.7% of the operating band (1.5-37 GHz). Port 2 (the red curve) has ARBWs of 2.45-2.6 GHz and 5.4-6.5 GHz, which are about 0.9% and 6% of the wide operating band 1.35-36 GHz. Port 3 (the blue curve) has wide ARBWs less than 3 dB at 4.8-15 GHz, which are approximately 36% of its operating band (1.3-30 GHz). Port 4 (the green curve) has an ARBW of 5.5-20 GHz, which is about 38% of its operating band (1.5-39) GHz. Therefore, the proposed antenna has CP characteristics at all ports with different ARBWs.

Figure 8a represents the left (black curve) and the right (red curve) polarized radiations for all ports at 5.7 GHz. The
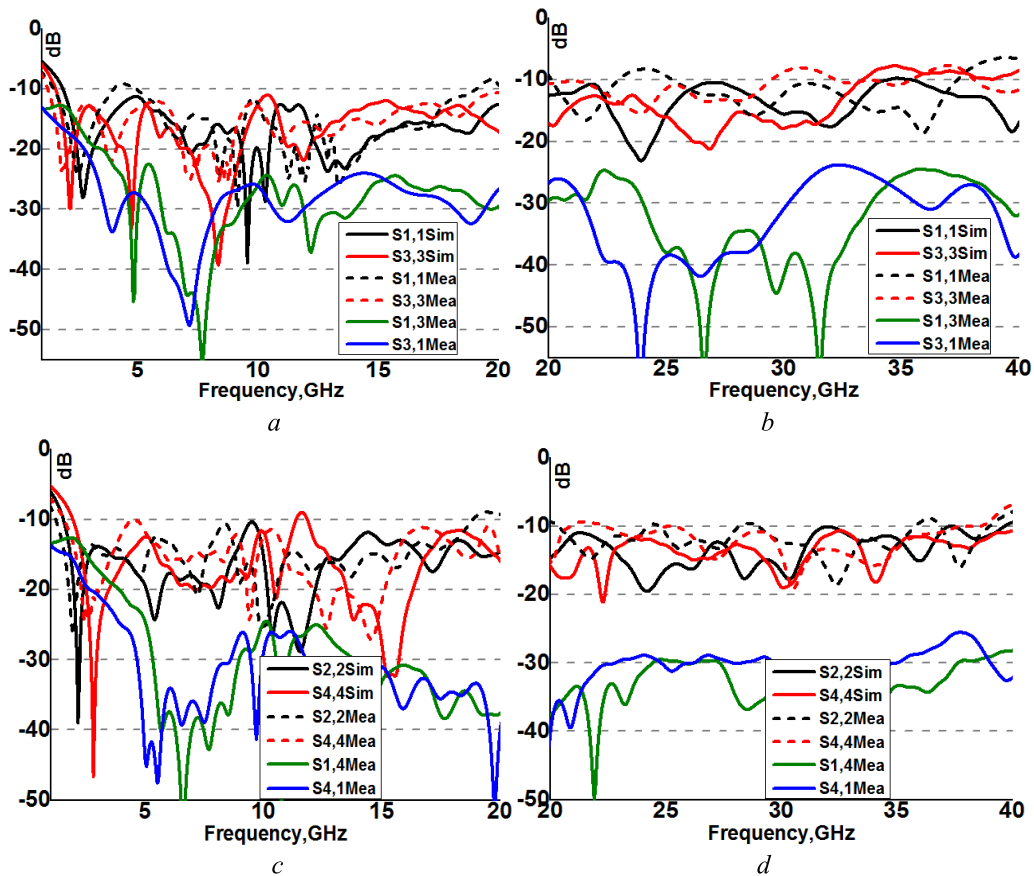
FIGURE 10. Measured and simulated S-parameters for all ports. a.S-parameters for port 1 and port 3 at (1.5-20) GHz. b. S-parameters for port 1 and port 3 at (20-40) GHz. c. S-parameters for port 2 and port 4 at (1.5-20) GHz. d. S-parameters for port 2 and port 4 at (20-40) GHz.

left and right radiation patterns at 5.7 GHz for all ports are nearly perpendicular to each other and match the values of ARBW in Figure7. In Figure 8b, the cross polarization and co-polarization for all ports are less than -20 dB.

The benefits of using Amer fractal slot structure in the design are providing many paths for the surface current to generate many resonant frequencies, which together achieve a wide operating band. The proposed antenna also has a low profile, low mutual coupling between opposite ports, CP radiation, and a compact size.

III. MEASURMENTS AND RESULTS

The prototype of the antenna is presented in Fig.9. The values of the S-parameters (dashed curves) and simulated data (solid curves) for all ports are presented in Fig.10 (The frequency band is divided into two sub-bands.). Given the impurity of certain materials used in the prototype and the impedance of the soldering and the connectors, some of the resonant frequencies in the measurement curves exhibit a shift relative to the simulated data in Figure 10.

However, Figure 10 shows good agreement between the simulated values (solid black and red curves) and measured values (dashed black and red curves) of reflection coefficients. The black dashed curves in Figures 10a and 10b show

wide dual-measured impedance bandwidths of 1.5-19.2 GHz and 25-37.2 GHz for port 1. Other results include a measured operating band for port 3 of 1.3-29 GHz (red dashed curves in Figures 10a and 10b); wide dual operating bands of 1.4-19 GHz and 20-35.5 GHz for port 2 (black dashed curve in Figures 10c and 10d); and dual operating bands of 1.6-21 GHz and 22-37 GHz for port 4 (red dashed curves in Figures 10c and 10d). The blue and green curves in Figure 10 indicate that the measured mutual coupling values between ports 1 and 3 or between ports 2 and 4 are less than -15 dB at 1.5-3 GHz and between -25 dB and -50dB at 3-30 GHz. Thus, the MIMO fractal slot antenna presented in this work shows a super wide operating band (nearly 1.5-30 GHz) and low mutual coupling between opposite ports.

The measured radiation patterns, gain, and efficiency for ports 1-3 and 2-4 nearly match. Hence, the succeeding portions focus on ports 1 and 3. Figure 11 depicts the normalized patterns for ports 1 and 3 at resonant frequencies of 1.8 GHz, 5.8 GHz, and 28 GHz. There is good agreement between the simulated and measured radiation patterns.

The patterns at the H-Plane for all resonant frequencies are all mostly omnidirectional, whereas the E-Patterns vary according to the resonant frequencies. The measured
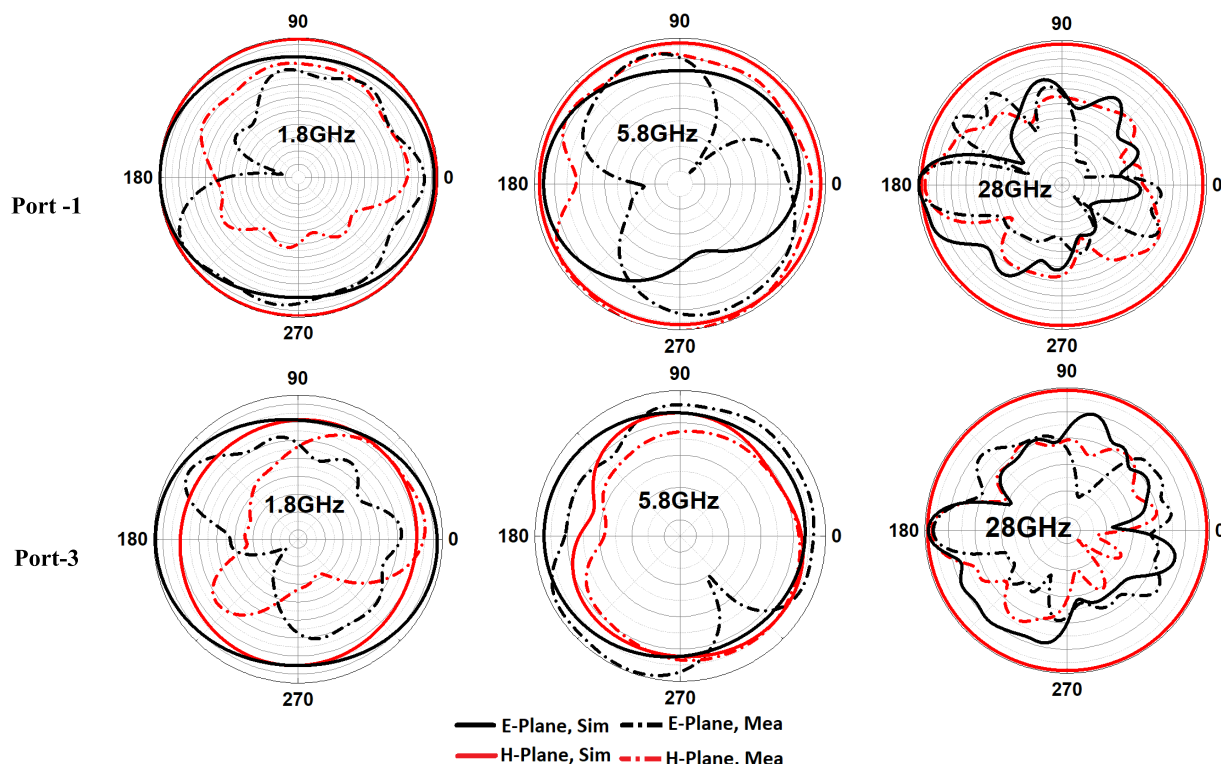
FIGURE 11. Normalized radiation patterns (Measured and simulated) in E-Plane and H-plane at 1.8GHz, 5.8GHz and 28GHz for Port-1 &3.

TABLE 2. compression between single [25] and MIMO Amer fractal slot antennas.

Specification	Single	MIMO
BW (GHz)	(4.4-6.1) (8.4-10.9) (13.1-13.7) (18.2-19)	P1 (1.5-19.2 & 25-37.2) P2 (1.4-19 & 20-35.5) P3 (1.4-29) P4 (1.6-21 & 22-37)
ARBW (GHz)	(9-10.1)	P1 (4.7-5.8) P2 (2.5-2.6 & 5.4-6.5) P3 (4-5.9) P4 (5.5-10)
Gain(dBi)	2.2-4.1	1-6.3
Efficiency (%)	85-94	50-85
Size (mm)	25 x 11.5 x 0.8	33 x 33 x 0.8
Application	Wi-Fi, WiMAX Only at 5 GHz band	3G, LTE (2.6 GHz/3.5 GHz), Wi-Fi (2.4 GHz/5 GHz), WiMAX (2.5 GHz/3.5 GHz/5 GHz), ISM (2.5 GHz/5 GHz) and 5G

radiation patterns in the E-Plane are bean-like in shape. At a resonant frequency of 5.8 GHz, the pattern in the E-plane has dual major lobes. At 28 GHz, there are many side lobes in the radiation patterns in the E-plane.

The efficiency of the antenna when port 1 is excited varies between 50% at 1.8 GHz and 85% at 30 GHz, as illustrated by the blue solid points in Figure 12a, For port 3, the efficiency reaches its maximum value (80%) at 15 GHz and its minimum value (54%) at 1.8 GHz (blue empty points in Figure 12a).The efficiency values of ports 2and 4 are almost the same as those of ports 1 and 3 (blue square points in Figure 12b).

The measured ARBW of the proposed antenna when port 1 is excited is 4.7-5.8 GHz, which is approximately 6% of the first operating band of 1.5-19.2 GHz, as illustrated by the black triangle points in Figure 12a. The black circle points in Figure 12a represent an ARBW of 4-5.9 GHz, which is about 6.8% of the operating band of 1.3-29 GHz when port 3 is excited. Port 2 has ARBWs of 2.5-2.6 GHz and 5.4-6.5, which are approximately 0.5% and 6.2% of the first operating band of 1.4-19 GHz (the black triangle points in Figure 12b).

Port 4 has a wide ARBW of 5.5-10 GHz, which is about 23% of the first operating band of 1.6-21 GHz (the black circle points in Figure 12b), a result of the perpendicular paths for the surface current near port 4.

Figure 13 shows that the proposed antenna has gain values between 1.3 and 6.3 dBi when port 1 is excited (black square points) and between 1 and 6.2 dBi when port 3 is excited (black triangle points). Port 2 has measured gain values between 1.2 and 6.3dBi (red circle points), while the measured gain values for port 4 are 1-6.3dBi (red triangle points).

TABLE 3. Comparison of the proposed antenna to previous MIMO fractal antennas.

Ant.	FBW %	Efficiency %	Gain (dBi)	ARBW (GHz)	Mutual Coupling(dB)	Size (mm)
[4]	2, 9	70-80	-	LP	< -25	77 x 34 x 0.8
[9]	5, 2, 3.7, 2.3, 0.5	-	2.5∼ 6.5	3.6-3.65	< -17	82 x 40x 0.8
[21]	95	56	-1 ∼ 3.1	2.2-3.2	< -30	8 x 8 x 0.8
[22]	14, 12, 4, 7	70-90	5 ∼9	LP	< -27	70 x 37 x 1.6
[23]	7	77-84	2 ∼6	LP	< -32	120 x 90 x 15
[24]	0.7	68	-	LP	< -40	68 x 40 x 1.6
This work	P1 (85, 19) P2 (86, 28) P3 (75, 51) P4 (91)	50-85 53-85 54-80 56-82	1.3 ∼6.3 1.2 ∼6.3 1 ∼6.2 1 ∼6.3	(4.7-5.8) (2.5-2.6) (5.4-6.5) (4-5.9) (5.5-10)	< -15 for 1.5-3GHz (opposite ports) $-25 \sim -50$ for 3-30GHz (opposite ports)	33 x 33 x 0.8

a

b

FIGURE 12. Measured AR and total efficiency for port 1&3,2 & 4.

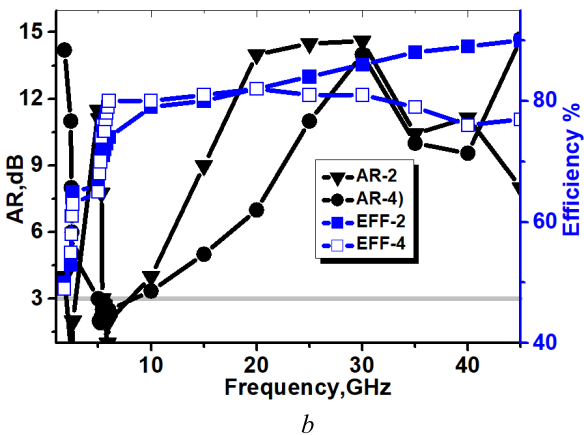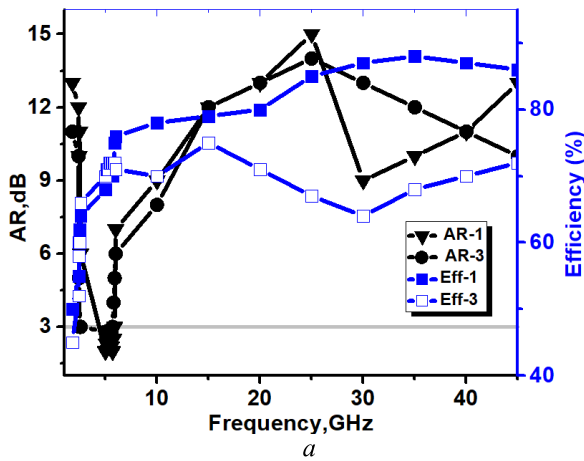**FIGURE 13.** Measured gain for ports 1 & 3.

Table-II is a comparison of the proposed MIMO antenna and the single-element antenna reported in [25]. The data in Table II indicate that the MIMO antenna has a larger surface area than does the single-element antenna in [25]. The former has many specifications, such as duplicated operating band; high gain (especially at high frequencies); and usability for modern communication applications, such as 3G, LTE (4G), all bands for WLAN/WiMAX, and 5G
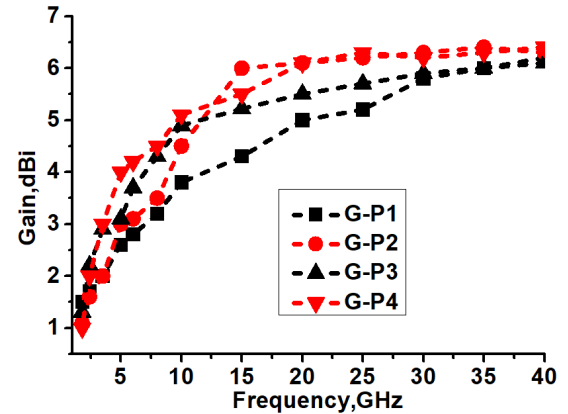
Table-III is a comparison of the measured radiation parameters of the MIMO Amer fractal antenna with the previous MIMO fractal antennas investigated in [4], [9], and [21]–[24]. Based on Table-III, none of the previous antennas has the impedance bandwidth at all ports to meet most market needs, such as 3G, LTE (2.6 GHz and 3.5 GHz bands), WLAN (2.4 GHz and 5 GHz bands), WiMAX (2.5 GHz, 3.5 GHz, and 5 GHz bands), ISM (2.4 GHz and 5 GHz bands) and 5G (5-6 GHz and 27-28 GHz bands). None of the previous antennas achieved acceptable gain and efficiency while maintaining a compact size.

The antenna in the current study has low mutual coupling between opposite ports (especially at 3-30 GHz); the CP characteristics at all ports with different values of ARBW (especially at the required spectrum – 5-6 GHz – which is used by many modern wireless communications such as Wi-Fi, WiMAX, ISM and 5G); a low profile; and acceptable gain values (1-6.3dBi).

IV. CONCLUSION

This study investigated a compact MIMO antenna with dual opposite ports. The design of the proposed MIMO used an

Amer fractal slot structure to provide multiple paths for the surface current, where each path creates its own resonant frequencies, which together achieve a wide operating band. Some of these paths are perpendicular to each other, which causes circular polarization characteristics, low mutual coupling between the opposite ports (1 and 3, 2 and 4) for all operating bands (nearly 1.5-30 GHz) and less than -10dB for all neighbor ports at frequency band (15-30 GHz). The measured efficiency varies between 50% and 85%, and low profile in compact size. Therefore, the antenna can support many wireless communication devices such as 3G, LTE (2.6/3.5 GHz), Wi-Fi (2.4/5 GHz), WiMAX (2.5/3.5/5 GHz), ISM (24/5 GHz), and 5G (5-6 GHz and 27-28 GHz).

REFERENCES

[1] A. T. Abed, *Fractal and Slot Antennas for Portable Communication Devices*. 1st ed. Saarbrücken, Germany: Lab Lamert for Acadmic puplication, 2019.

[2] K. Ding, C. Gao, D. Qu, and Q. Yin, "Compact broadband MIMO antenna with parasitic strip," *IEEE Antennas Wireless Propag. Lett.*, vol. 16, pp. 2349–2353, 2017.

[3] Y. Sharma, D. Sarkar, K. Saurav, and K. Srivastava, "Three-element MIMO antenna system with pattern and polarization diversity for WLAN applications," *IEEE Antennas Wireless Propag. Lett.*, vol. 16, pp. 1163–1166, 2017.

[4] M. V. Komandla, G. Mishra, and S. K. Sharma, "Investigations on dual slant polarized cavity-backed massive MIMO antenna panel with beamforming," *IEEE Trans. Antennas Propag.*, vol. 65, no. 12, pp. 6794–6799, Dec. 2017.

[5] A. Peristerianos, A. Theopoulos, A. G. Koutinos, T. Kaifas, and K. Siakavara, "Dual-band fractal semi-printed element antenna arrays for MIMO applications," *IEEE Antennas Wireless Propag. Lett.*, vol. 15, pp. 730–733, 2016.

[6] S. S. Jehangir and M. S. Sharawi, "A miniaturized UWB biplanar yagi-like MIMO antenna system," *IEEE Antennas Wireless Propag. Lett.*, vol. 16, pp. 2320–2323, 2017.

[7] R. Hussain, A. Ghalib, and M. S. Sharawi, "Annular slot-based miniaturized frequency-agile MIMO antenna system," *IEEE Antennas Wireless Propag. Lett.*, vol. 16, pp. 2489–2492, 2017.

[8] A. Ghalib and M. S. Sharawi, "TCM analysis of defected ground structures for MIMO antenna designs in mobile terminals," *IEEE Access*, vol. 5, pp. 19680–19692, 2017.

[9] S.-J. Park, M.-H. Jeong, K.-B. Bae, D.-C. Kim, L. Minz, and S.-O. Park, "Performance comparison of 2 × 2 MIMO antenna arrays with different configurations and polarizations in reverberation chamber at millimeterwaveband," *Trans. Antennas Propag.*, vol. 65, no. 12, pp. 6669–6678, Dec. 2017.

[10] S. Rajkumar, N. V. Sivaraman, S. Murali, and K. T. Selvan, "Heptaband swastik arm antenna for MIMO applications," *IET Microw., Antennas Propag.*, vol. 11, no. 9, pp. 1255–1261, Jul. 2017.

[11] M. S. Khan, A.-D. Capobianco, A. Iftikhar, Raed M. Shubair, D. E. Anagnostou, and B. D. Braaten, "Ultra-compact dual-polarised UWB MIMO antenna with meandered feeding lines," *IET Microw., Antennas Propag.*, vol. 11, no. 7, pp. 997–1002, Jun. 2017.

[12] M. Akbari, H. A. Ghalyon, M. Farahani, A.-R. Sebak, and T. A. Denidni "Spatially decoupling of CP antennas based on FSS for 30-GHz MIMO systems," *IEEE Access*, vol. 5, pp. 6527–6537, 2017.

[13] D. Sipal, M. P. Abegaonkar, and S. K. Koul, "Easily extendable compact planar UWB MIMO antenna array," *IEEE Antennas Wireless Propag. Lett.*, vol. 16, pp. 2328–2331, 2017.

[14] J. Y. Deng, J. Li, L. Zhao, and L. Guo, "A dual-band inverted-F MIMO antenna with enhanced isolation for WLAN applications," *IEEE Antennas Wireless Propag. Lett.*, vol. 16, pp. 2270–2273, Jun. 2017.

[15] A. Ramachandran, S. Mathew, V. Rajan, and V. Kesavath, "A compact triband quad-element MIMO antenna using SRR ring for high isolation," *IEEE Antennas Wireless Propag. Lett.*, vol. 16, pp. 1409–1412, 2016.

[16] R. Hussain, A. T. Alreshaid, S. K. Podilchak, and M. S. Sharawi, "Compact 4G MIMO antenna integrated with a 5G array for current and future mobile handsets," *IET Microw., Antennas Propag.*, vol. 11, no. 2, pp. 271–279, 2017.

[17] G. Li, H. Zhai, Z. Ma, C. Liang, R. Yu, and S. Liu, "Isolation-improved dual-band MIMO antenna array for LTE/WiMAX mobile terminals," *IEEE Antennas Wireless Propag. Lett.*, vol. 13, pp. 1128–1131, 2014.

[18] C.-X. Mao and Q.-X. Chu, "Compact coradiator UWB-MIMO antenna with dual polarization," *IEEE Trans. Antennas Propag.*, vol. 62, no. 9, pp. 4474–4480, Sep. 2014.

[19] A. Toktas and A. Akdagli, "Wideband MIMO antenna with enhanced isolation for LTE, WiMAX and WLAN mobile handsets," *Electron. Lett.*, vol. 50, no. 10, pp. 723–724, May 2014.

[20] G. Brzezina, A. A. Ghasemi, J. Sydor, and A. Vukovic, "Design and analysis of a low-profile directive antenna array for multi-element terminals," *IET Microw., Antennas Propag.*, vol. 18, no. 8, pp. 611–620, Jun. 2014.

[21] A. T. Abed, "Highly compact size serpentine-shaped multiple-input–multiple-output fractal antenna with CP diversity," *IET Microw., Antennas Propag.*, vol. 12, no. 4, pp. 636–640, Mar. 2018.

[22] M. Alibakhshikenari, M. Khalily, B. S. Virdee, C. H. See, R. A. Abd-Alhameed, and E. Limiti, "Mutual coupling suppression between two closely placed microstrip patches using EM-bandgap metamaterial fractal loading," *IEEE Access*, vol. 7, pp. 23606–23614, 2019.

[23] M. Alibakhshikenari, B. S. Virdee, C. H. See, R. Abd-Alhameed, A. H. Ali, F. Falcone, and E. Limiti, "Study on isolation improvement between closely-packed patch antenna arrays based on fractal metamaterial electromagnetic bandgap structures," *IET Microw., Antennas Propag.*, vol. 12, no. 14, pp. 2241–2247, Nov. 2018.

[24] A. H. Radhi1, R. Nilavalan, Y. Wang, H. Al-Raweshidy, A. A. Eltokhy, and N. A. Aziz, "Mutual coupling reduction with a novel fractal electromagnetic bandgap structure," *IET Microw., Antennas Propag.*, vol. 13, no. 2, pp. 134–141, Feb. 2019.

[25] A. T. Abed, M. S. J. Singh, and M. T. Islam, "Amer fractal slot antenna with quad operating bands high efficiency for wireless communications," in *Proc. IEEE 3rd Int. Symp. Telecommun. Technol. (ISTT)*, Kuala Lumpur, Malaysia, Nov. 2016, pp. 6–8.

[26] H. Li, X. Lin, B. K. Lau, and S. Hel, "Equivalent circuit based calculation of signal correlation in lossy MIMO antennas," *IEEE Trans. Antennas Propag.*, vol. 61, no. 10, pp. 5214–5222, Oct. 2013.

AMER TAWFEEQ ABED received the B.Sc. degree in electrical engineering from the College of Engineering, University of Baghdad, in 1984, the master's degree in communication engineering from the University of Tenaga, Malaysia, and the Ph.D. degree from UKM. He is currently a Lecturer with the Communication Engineering Department, Al-Ma'moon University College, Baghdad. He has wide experience in designing the RF circuit and antenna field. He has published 25 articles in ISI journals and two books about antenna design. He is a member of the European Microwave Association (EMA). He has reviewed more than 40 articles in IET and the IEEE journals.

AQEEL MAHMOOD JAWAD received the B.Sc. degree in computer and communication engineering from Al-Rafidain University College, Iraq, in 2009, and the M.Sc. degree in electrical engineering from Universiti Tenaga National (UNITEN), Malaysia, in 2014. He is currently pursuing the Ph.D. degree with the Department of Electrical, Electronics, and Systems Engineering, Faculty of Engineering and Built Environments, Universiti Kebangsaan Malaysia. He is currently with the Department of Computer and Communication Engineering, Al-Rafidain University College, Baghdad, Iraq, as a Lecturer.

• • •